Results in Physics 6 (2016) 7–11

Contents lists available at ScienceDirect

Results in Physics

journal homepage: www.journals.elsevier.com/results-in-physics

Prominent spectral features of Sm^{3+} ion in disordered zinc tellurite glass

Y.A. Tanko, M.R. Sahar *, S.K. Ghoshal

Advanced Optical Materials Research Group, Department of Physics, Faculty of Science, Universiti Teknologi Malaysia, 81310 Skudai, Johor, Malaysia

ARTICLE INFO

Article history:
Received 16 September 2015
Accepted 2 December 2015
Available online 11 December 2015

Keywords:
Tellurite glass
Samarium oxide
FTIR spectroscopy
Absorption
Emission

ABSTRACT

Trivalent rare earth doped glasses with modified spectroscopic features are essential for solid state lasers and diverse photonic applications. Glass composition optimisation may fulfil such demand. Stimulating the spectral properties of samarium (Sm^{3+}) ions in tellurite glass host with desired enhancement is the key issue. Glasses with composition $(80-x)TeO_2$–$20ZnO$–$(x)Sm_2O_3$, where $0 \leqslant x \leqslant 1.5$ mol% are prepared using melt quenching method. The role of varying Sm^{3+} contents to improving the absorption and emission properties of the prepared glasses are determined. XRD pattern verifies amorphous nature of synthesised glasses. FTIR spectroscopy has been used to observe the structural modification of (TeO_4) trigonal bipyramid structural units. DTA traces display prominent transition peaks for glass transition, crystallisation and melting temperature. Samples are discerned to be stable with desired Hruby parameter and superior glass forming ability. The UV–Vis–NIR absorption spectra reveals nine peaks centred at 470, 548, 947, 1085, 1238, 1385, 1492, 1550 and 1589 nm. These bands arise due to $^6H_{5/2} \rightarrow {}^4I_{11/2}$, $^4G_{5/2}$, $^6F_{11/2}$, $^6F_{9/2}$, $^6F_{7/2}$, $^6F_{5/2}$, $^6F_{3/2}$, $^6H_{15/2}$ and $^6F_{1/2}$ transitions, respectively. The direct, indirect band gap and Urbach energy calculated from the absorption edge of UV–Vis–NIR spectra are found to appear within (2.75–3.18) eV, (3.22–3.40) eV, and (0.20–0.31) eV, respectively. The observed increase in refractive index from 2.45 to 2.47 is ascribed to the generation of non-bridging oxygen atoms via the conversion of TeO_4 into TeO_3 units. Conversely the decrease in refractive index to 2.39 is attributed to the lower ionic radii (1.079 Å) of Sm^{3+}. PL spectra under the excitation of 452 nm display four emission bands centred at 563, 600, 644 and 705 nm corresponding to $^4G_{5/2} \rightarrow {}^6H_{5/2}$, $^6H_{7/2}$, $^6H_{9/2}$ and $^6H_{11/2}$ transitions of samarium ions. Excellent features of the results nominate these compositions towards prospective applications.

Introduction

Over the years, rare earth doped oxide glasses has proven to be attractive for making solid state lasers, optical fibres, optical amplifiers and colour display devices [1–4]. Tellurite glasses are oxide glasses with TeO_2 as their major constituents and a number of works have been reported by other researchers on tellurite glasses [2,5,6]. Among the oxide glasses, tellurite is considered to be more potential due to its notable features including low phonon energy (700–800 cm^{-1}), high thermal and chemical stability, high refractive index ($\geqslant$2.0), wide infrared transmission (0.3–6.0 μm), and low melting point (~800 °C) [3,5,7–11]. However, glass forming ability of tellurite dioxide is decided by the proportion of modifiers such as ZnO, MgO, Na_2O, etc. Actually, the easy breaking of weak Te–O bond in tellurite dioxide through the incorporation of rare earth atom and heavy metals facilitates the formation of glass network. It is acknowledged that Sm^{3+} doped glasses possess great emission band which originates from $^4G_{5/2} \rightarrow {}^6H_J$ (J = 5/2, 7/2, 9/2, 11/2) transitions. Intensity of these bands is strongly guided by the Sm^{3+} concentration [12]. The structural arrangements in tellurite glasses are being investigated by Infrared and Raman spectroscopies. Two basic structural units exist in TeO_2 as TeO_4 trigonal bipyramid (tbp) and TeO_3 trigonal pyramid (tp) [13–16]. Despite much research, better improvement in the structural, thermal and optical properties of Sm^{3+} doped zinc tellurite glass is not clearly understood.

In the present work, zinc tellurite glass doped with Sm^{3+} is prepared using the conventional melt quenching method. The FTIR analysis is performed for structural characteristics, DTA for thermal features. While UV–vis absorption and photoluminescence spectroscopy are performed for optical characterisation. The influence of Sm^{3+} on the structural, thermal and optical features are demonstrated.

Materials and methods

Glasses of chemical composition $(80-x)TeO_2$–$20ZnO$–xSm_2O_3 with $0 \leqslant x \leqslant 1.5$ mol% are prepared using conventional

* Corresponding author.
E-mail address: mrahim057@gmail.com (M.R. Sahar).

http://dx.doi.org/10.1016/j.rinp.2015.12.001
2211-3797/

melt-quenching technique. About 20 g of the analytical grade raw materials of tellurium dioxide (Sigma–Aldrich 99%), zinc oxide (ACROS 99%) and samarium oxide (Sigma–Aldrich 99.99%) are weighted and thoroughly grounded. Then, the powders are melted into an alumina crucible by a raising heat electronic furnace at 800 °C for 30 min. Upon complete melting and desired viscosity attainment, the melt is poured between two preheated steel molds in an alternative furnace and kept for 3 h at 250 °C. Finally, the samples are cooled down slowly to the room temperature, cut into preferred sizes and polished for superior transparency. The nominal compositions of the prepared glasses and their corresponding codes together with some of their physical properties are listed in Table 1.

The density (ρ) of each sample is measured by Archimedes method using toluene as the immersion liquid with an estimated error of ±0.002. The density of each sample is determined by the relation

$$\rho = \rho_L \frac{W_L}{W_L - W_W} \quad (1)$$

where ρ_L is the density of toluene (0.8669 g cm^{-3}), W_L and W_w are the sample weights in air and toluene respectively. The molar volume V_m is calculated from the relation [17]

$$V_m = \sum \frac{x_i M_i}{\rho} \quad (2)$$

x_i and M_i represent molar fraction and molecular weight of ith component of the sample respectively. Makishima and Mackenzie [18,19] measured the ionic parking density (V_t) from the relation

$$V_t = \left(\frac{1}{V_m}\right) \sum (V_i x_i) \quad (3)$$

where x_i is the mole fraction (mol%) and V_i represents the packing density parameter (m^3 mol^{-1}). For an oxide glass of the form M_xO_y, the value of V_i is estimated from the relation [19]

$$V_i = \left(\frac{4\pi N_A}{3}\right)[Xr_M^3 + Yr_o^3] \quad (4)$$

where N_A is Avogadro's number (mol^{-1}) and r_M and r_0 represent the Shannon's ionic radius of metal and oxygen respectively.

X-ray diffraction technique is carried out using a Bruker D8 Advance diffractometer with Cu-Kα radiations (λ = 1.54 Å) operated at 40 kV and 100 mA. The XRD data of powdered samples are collected in the range of 2θ = 10–80° at scanning rate of 0.05°/s. Thermal properties are determined using a differential thermal analyser (Pyris Diamond TG-DTA, Japan). The room temperature absorption spectra in the wavelength range of 200–1800 nm are recorded using Shimadzu 3101PC spectrophotometer. A Perkin-Elmer LS-55 luminescence spectrometer attached with a Xenon lamp as excitation source is employed for room temperature emission measurement.

Table 1
Nominal composition of glasses with codes, density (g cm^{-3}), molar volume (V_m) and ionic packing density (V_t).

Glass codes	Mol%			ρ (g cm^{-3})	V_m (cm^3 mol^{-1})	V_t
	TeO_2	ZnO	Sm_2O_3			
TZS0	80.0	20	0.0	5.571	25.84	0.4922
TZS1	79.7	20	0.3	5.578	25.91	0.4923
TZS2	79.4	20	0.6	5.585	25.98	0.4923
TZS3	79.1	20	0.9	5.599	26.01	0.4932
TZS4	78.8	20	1.2	5.608	26.07	0.4935
TZS5	78.5	20	1.5	5.613	26.15	0.4934

Results and discussions

Fig. 1 shows the XRD pattern of the prepared glasses in the range of 2θ = 10–80°. Complete absence of any discrete or continuous sharp peak and the presence of broad hunch in the diffraction pattern confirms the amorphous nature of these samples [20].

Fig. 2 shows the variation of Sm_2O_3 concentration plotted against density and molar volume of the prepared glass. The density and molar volume increases with the increasing concentration of Sm_2O_3 which indicates an increase of glass network rigidity. The increase in glass density is due to an increase in the number of bridging oxygen in the glass [21–23]. Moreover, the increase in molar volume results in an increase in the bond length or the interatomic spacing [24].

The IR spectroscopy gives the vibrational spectra of the glass and Fig. 3 shows the Fourier transform infrared (FTIR) spectra for the sample glass. Table 2 summarises the band assignment as evidenced by the observed peaks. The band that occurs at around 634–653 cm^{-1} and 759–774 cm^{-1} are attributed to Te–O vibration in TeO_4 and TeO_3 structural units respectively [25,26]. It is observed that the transmission intensity changes with varying concentration of Sm^{3+} in the glass composition.

Fig. 4 displays the DTA thermo-grams of prepared glass with sharp endothermic peak corresponding to melting temperature (T_m). The onset of crystallisation (T_c) is manifested through a prominent exothermic peak and tiny peaks for the glass transition (T_g) temperature. Table 3 summarises the values of T_g, T_c, T_m, glass stability (S) and Hruby parameter (H) for the synthesised glass samples.

The slight decrease of glass stability factor S (T_c–T_g) with the increase of Sm^{3+} ion contents (0.6 mol%) is likely due to the decrease in rigidity of the glass network [27,28]. Further increase of the Sm^{3+} concentration leads to an increase in the network rigidity as well as stability of glasses. Hruby parameter H is used in estimating the stability of the prepared glass from the relation [29].

$$H = \frac{T_C - T_g}{T_m - T_C} \quad (5)$$

For larger values of H, the stability of the glass formed is higher [29]. The occurrence of two crystallisation peaks are presumably because of different crystallisation phases for all samples as reported [30].

The absorption spectra recorded in the wavelength range of 400–1800 nm as shown in Fig. 5 are comprised of prominent bands centred at 470, 548, 947, 1085, 1238, 1385, 1492, 1550 and 1589 nm, allocated to the transitions of $^6H_{5/2} \rightarrow {}^4I_{11/2}$, $^4G_{5/2}$, $^6F_{11/2}$, $^6F_{9/2}$, $^6F_{7/2}$, $^6F_{5/2}$, $^6F_{3/2}$, $^6H_{15/2}$ and $^6F_{1/2}$, respectively. These bands originated from electric dipole transition ($\Delta J \leqslant 6$) and magnetic

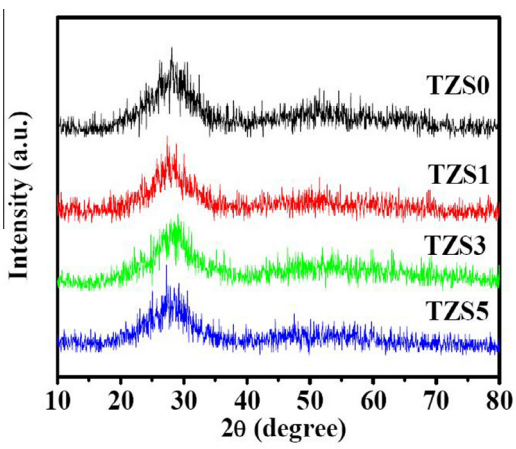

Fig. 1. Typical XRD pattern of Sm^{3+} doped zinc tellurite glasses.

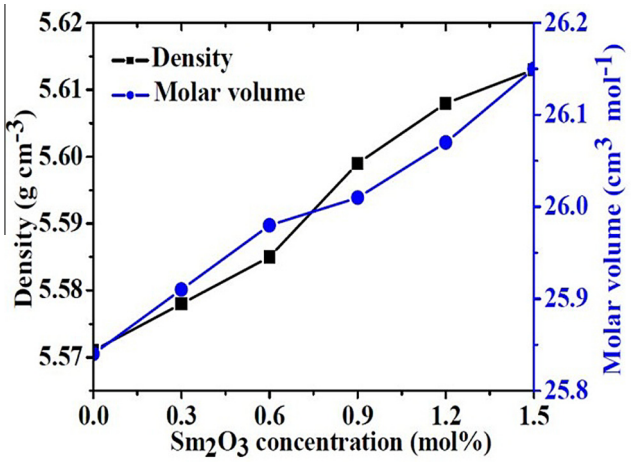

Fig. 2. Sm_2O_3 concentration dependent variation of glass density and molar volume.

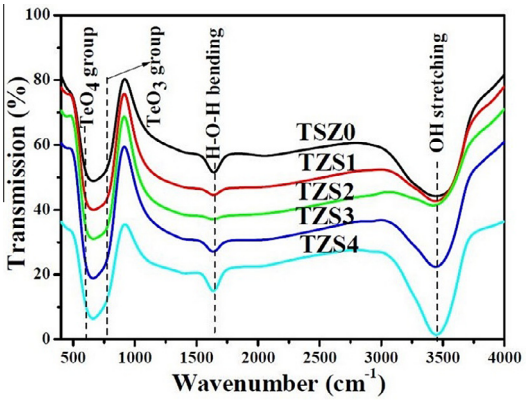

Fig. 3. FTIR spectra of glass samples in the range of 450–4000 cm^{-1}.

Table 2
Absorption peaks of the FTIR spectra for the glass sample.

Sample codes	Absorption peaks (cm^{-1})			
TZS0	634	759	1646	3454
TZS1	644	767	1646	3454
TZS2	653	774	1646	3454
TZS3	653	774	1646	3470
TZS4	653	774	1646	3454

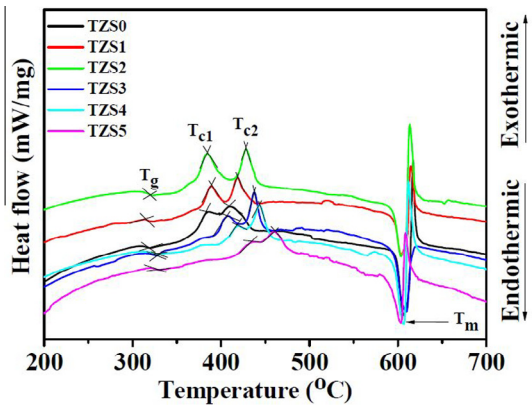

Fig. 4. DTA curves of Sm^{3+} doped zinc tellurite glasses.

Table 3
Sm_2O_3 concentration dependent thermal properties of studied glasses.

Glass	T_g (°C)	T_{c1} (°C)	T_{c2} (°C)	T_m (°C)	S = T_{c1}–T_g (°C)	H
TZS0	319	383	408	605	64	0.29
TZS1	314	389	418	603	75	0.35
TZS2	320	384	428	603	64	0.29
TZS3	327	407	437	608	80	0.40
TZS4	328	418	444	605	90	0.48
TZS5	329	434	460	603	105	0.62

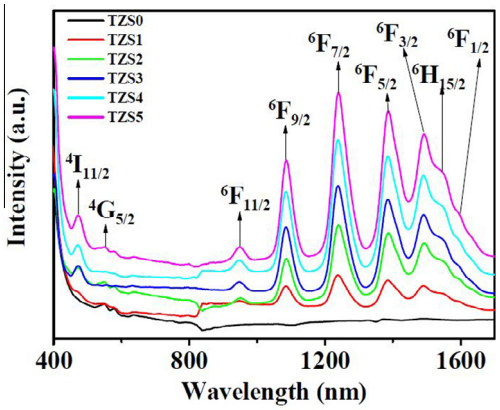

Fig. 5. Sm^{3+} ion contents dependent absorption spectra of synthesised glasses.

Table 4
Energy for direct (E^D_{opt}, eV) and indirect (E^I_{opt}, eV) band gaps; Urbach energy (ΔE, eV), and refractive index (n) of prepared glasses.

Glass	E^D_{opt}	E^I_{opt}	ΔE	n
TZS0	2.80	3.22	0.26	2.45
TZS1	2.75	3.25	0.31	2.47
TZS2	3.16	3.37	0.20	2.36
TZS3	3.18	3.40	0.23	2.35
TZS4	3.10	3.36	0.21	2.37
TZS5	3.04	3.32	0.23	2.39

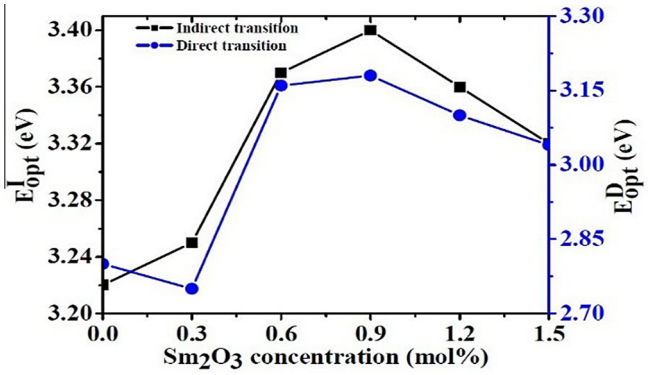

Fig. 6. Indirect (E^I_{opt}) and direct (E^D_{opt}) optical band gap against Sm_2O_3 concentration.

dipole transition ($\Delta J = 0, \pm 1$) [31,32]. Generally, trivalent Sm^{3+} ions in a host are categorised into low (band up to ~930 nm) and high (in the range ~570–310 nm) transitions band [33]. The complete disappearance of some absorption transitions are due to the

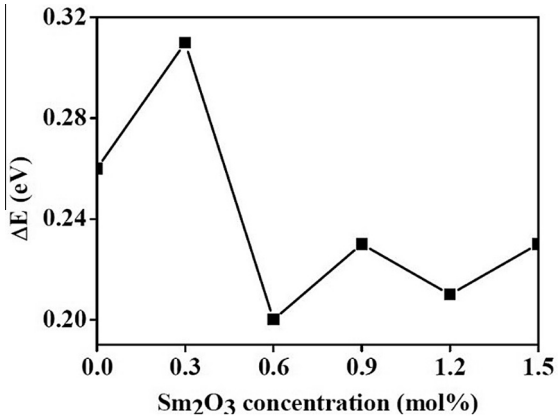

Fig. 7. Sm_2O_3 concentration dependent Urbach energy.

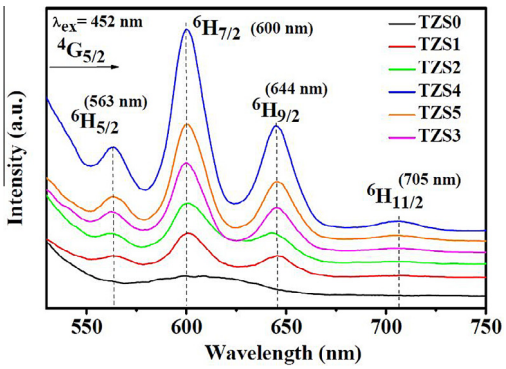

Fig. 8. Luminescence spectra for Sm_2O_3 doped zinc tellurite glasses.

presence of the modifier [32]. The UV–Vis absorption edge is further used to calculate the optical energy band gap for both direct and indirect transitions together with the Urbach energy as summarised in Table 4.

Davis and Mott theory [34] is used to determine the direct and indirect optical energy band gap using the value of absorption coefficient (α) of prepared samples from the UV–vis absorption spectra. The optical energy band gap is related to the absorption coefficient (α) via,

$$\alpha(v) = \frac{B(hv - E_{opt})^r}{hv} \tag{6}$$

where B is a constant, h is the photon energy, and E_{opt} is the optical energy band gap. Here the index $r = ½$ for direct allowed optical transition and $r = 2$ for indirect allowed transition [35].

The absorption coefficient is obtained using,

$$\alpha(v) = 2.303\frac{A}{t} \tag{7}$$

where A is the absorbance and t is the thickness of the sample.

The degree of disorder in amorphous and crystalline material is described by Urbach energy (ΔE) and is calculated using the relation,

$$\alpha(v) = B\exp\left(\frac{hv}{\Delta E}\right) \tag{8}$$

where B is constant.

Fig. 6 demonstrates the Sm_2O_3 concentration dependent variation of direct and indirect energy band gaps. Both direct and indirect optical band gap energies are found to increase with the increase in Sm_2O_3 concentration up to 0.9 mol% and decrease thereafter. This widening in the gap energy is attributed to the generation of large number of non-bridging oxygen (NBO) which are more covalent in character than the bridging oxygen [36]. Consequently, transfer of electrons from the valence band to the conduction band becomes easier.

Value of Urbach energy (Fig. 7) first increased with an increase of Sm_2O_3 concentration and then decreased. This indicates a rapid increase of long range order in the glass. The glasses having low Urbach energy would have lower disorder and hence less brittle, but weak bonds are less likely to be turned into defects [37].

Fig. 8 illustrates the room temperature luminescence spectra of prepared samples in the wavelength range of 530–750 nm under 452 nm excitations. The spectra comprised of four significant emission bands centred at 563 (moderate green), 600 (intense orange), 644 (moderate red) and 705 nm (weak red). These bands are assigned to $^4G_{5/2} \rightarrow {}^6H_{5/2}$, $^6H_{7/2}$, $^6H_{9/2}$ and $^6H_{11/2}$ transitions, respectively [38]. Following the selection rule, $^4G_{5/2} \rightarrow {}^6H_{5/2}$ and $^4G_{5/2} \rightarrow {}^6H_{7/2}$ transitions are electric and magnetic dipole in nature while $^4G_{5/2} \rightarrow {}^6H_{11/2}$ and $^4G_{5/2} \rightarrow {}^6H_{11/2}$ transitions are purely electric dipole in nature.

The emission intensity is found to increase up to 1.2 mol% of Sm^{3+} contents and then displayed concentration quenching. The effect of concentration quenching with the increase in Sm^{3+} concentration leads to a decrease in inter-ionic separation, which is responsible for higher energy transfer among Sm^{3+} ions [39]. From the ground state $^6H_{5/2}$, ground state absorption (GSA) takes place which leads to the excitation of electrons to the excited energy level as shown in Fig. 9(a). Electron vibrational relaxation then

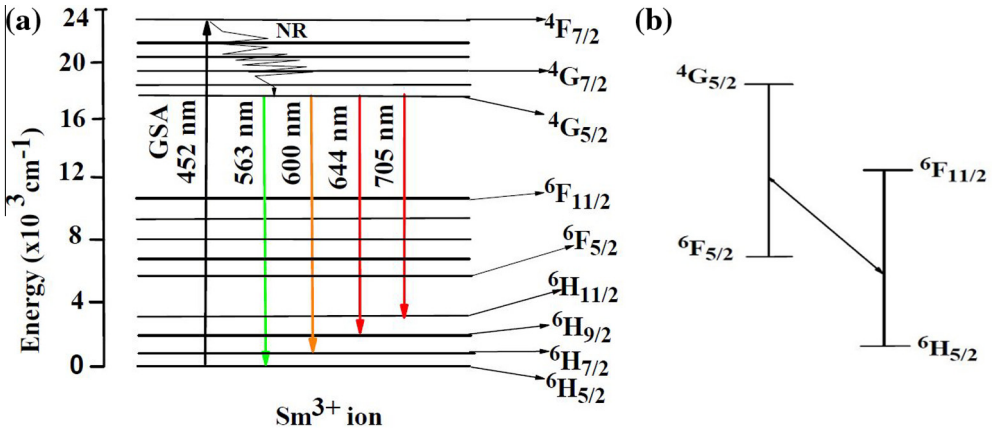

Fig. 9. (a) The possible energy level diagram of Sm^{3+} ion in zinc tellurite glass. (b) Cross relaxation.

occurs between the excited energy levels following Kasha's rule and a fast non-radiative (NR) decay takes place through cross relaxation process (Fig. 9(b)). This is followed by transition of electrons to the lowest excited energy level $^6H_{5/2}$ and then the excited electron will fall back to $^6H_{5/2}$, $^6H_{7/2}$, $^6H_{9/2}$, and $^6H_{11/2}$ with emission of green, orange and red fluorescence as in Fig. 9(a).

Conclusion

A series of Sm_2O_3 doped zinc-tellurite glasses are prepared by melt quenching method. The amorphous nature of the glass is confirmed by XRD analysis. Glasses are found to be thermally stable and transparent. Glass density is varied in the range of 5.571–5.613 g cm^{-3} and the molar volume is found to lie between 25.84–26.15 m^3 mol^{-1} respectively. The structural units TeO_4, TeO_{3+1} polyhedral or TeO_3 trigonal pyramid groups are located at 637–653 cm^{-1} and 759–774 cm^{-1} respectively. Thermal properties such as the temperature for glass transition, crystallisation and melting, stability and glass forming ability are determined from DTA analysis. The stability factor S is found in the range 64–105 °C which indicates an increasing stability with addition of Sm_2O_3 concentration. Absorption spectra displayed nine bands originating from electric dipole ($\Delta J = \leqslant 6$) and magnetic dipole ($\Delta J = 0, \pm 1$) transitions. Both direct (2.75–3.18) eV and indirect (3.22–3.40) eV optical band gap energies are increased with the increase in samarium ion concentration. The luminescence spectra exhibited four prominent peaks in the green, red and orange wavelength regions. Our results may contribute towards the development of tellurite glass based solid state lasers.

Acknowledgment

The authors gratefully acknowledge the financial support from UTM and Malaysian Ministry of Education through Vot.05H36, 05H45 (GUP) and 4F319, 4F424 (FRGS).

References

[1] Wei K, Machewirth DP, Wenzel J, Snitzer E, Sigel Jr GH. Opt Lett 1994;19:904.
[2] Wang JS, Vogel EM, Snitzer E. Opt Mater 1994;3:187.
[3] Jha A, Richards B, Jose G, Teddy-Fernandez T, Joshi P, Jiang X, Lousteau J. Prog Mater Sci 2012;57:1426.
[4] Mori A, Ohishi Y, Sudo S. Electron Lett 1997;33:863.
[5] El-Mallawany RAH. Tellurite Glasses Handbook: Physical Properties and Data. CRC Press; 2002.
[6] Fortes LM, Santos LF, Goncalves MC, Almeida RM, Mattarelli M, Montagna M, Chiasera A, Ferrari M, Monteil A, Choussedent S, Righini GC. Opt Mater 2007;29:503.
[7] Shin YB, Jang JN, Heo J. Opt Quantum Electron 1995;27:379.
[8] Murugan GS, Ohishi Y. J Non-Cryst Solids 2004;341:86.
[9] Jose R, Suzuki T, Ohishi Y. J Non-Cryst Solids 2006;352:5564.
[10] Murugan GS, Suzuki T, Ohishi Y. Appl Phys Lett 2005;86:221109.
[11] Lezal D, Pedlikova J, Kostka P, Bludska J, Poulain M, Zavadil J. J Non-Cryst Solids 2001;284:288.
[12] Jamalaiah BC, Kumar JS, Babu AM, Suhasini T, Moorthy LR. J Lumin 2009;129:363.
[13] Rao KJ, Bhat MH. Phys Chem Glasses 2001;42:255.
[14] Dimitriev Y, Bart JCJ, Dimitrov V, Arnaudov M. Z Anorg Allg Chem 1981;479:229.
[15] Jaba N, Mermet A, Duval E, Champagnon B. J Non-Cryst Solids 2005;351:833.
[16] Karthikeyan P, Suthanthirakumar P, Vijayakumar R, Marimuthu K. J Mol Struct 2015;1083:268.
[17] El-Diasty F, Abdel Wahab FA, Abdel-Baki M. J Appl Phys 2006;100:093511.
[18] Makishima A, Mackenzie JD. J Non-Cryst Solids 1973;12:35.
[19] Ahmmad Sk, Samee MA, Edukondalu A, Rahman S. Results Phys 2012;2:175.
[20] Babu P, Jin Seo Hyo, Kesavulu CR, Hyuk Jang Kyoung, Jayasankar CK. J Lumin 2009;129:444.
[21] Reddy MR, Kumar VR, Veeraiah N, Rao BA. Indian J Pure Appl Phys 1995;33:48.
[22] Eraiah B. Bull Mater Sci 2006;29:375.
[23] Arunkumar S, Marimuthu K. J Alloys Compd 2013;565:104.
[24] Hager IZ, El-Mallawany R. J Mater Sci 2009;45:897.
[25] Gowda VCV, Reddy CN, Radha KC, Anavekar RV, Etourneau J, Rao KJ. J Non-Cryst Solids 2007;353:1150.
[26] Rada S, Dehelean A, Culea E. J Non-Cryst Solids 2011;357:3070.
[27] Sahar MR, Sulhadi K, Rohani MS. J Non-Cryst Solids 2008;354:1179.
[28] Nawaz F, Rahim Sahar Md, Ghoshal SK, Asmahani Awang, Ahmed I. Phys B: Condens Matter 2014;433:89.
[29] Hruby A. Czech J Phys B 1972;22:1187.
[30] Nukui A, Taniguchi T, Miyata M. J Non-Cryst Solids 2001;293:255.
[31] Jayasimhadri M, Eun-Jin Cho, Ki-Wan Jang, Ho Sueb Lee, Sun Il Kim. J Phys D: Appl Phys 2008;41:175101.
[32] Mohan Babu A, Jamalaiah BC, Suresh Kumar J, Sasikala T, Rama Moorthy L. J Alloys Compd 2011;509:457.
[33] Boehm L, Reisfeld R, Spector N. J Solid State Chem 1979;28:75.
[34] Davis EA, Mott NF. Philos Mag 1970;22:903.
[35] Al-Ani SKJ, Higazy AA. J Mater Sci 1991;26:3670.
[36] Rajyasree C, Rao DK. J Non-Cryst Solids 2011;357:836.
[37] Gayathri Pavani P, Sadhana K, Chandra Mouli V. Phys B: Condens Matter 2011;406:1242.
[38] Reza Dousti M, Ghoshal SK, Amjad Raja J, Sahar MR, Arifin R. Opt Commun 2013;300:204.
[39] Bolundut L, Culea E, Borodi G, Stefan R, Munteanu C, Pascuta P. Ceram Int 2015;41:2931.